Journal of Nuclear Materials 516 (2019) 289–296

Contents lists available at ScienceDirect

Journal of Nuclear Materials

journal homepage: www.elsevier.com/locate/jnucmat

Strength and plasticity of amorphous silicon oxycarbide

Kaisheng Ming [a, b], Chao Gu [a, c], Qing Su [a], Yongqiang Wang [d], Arezoo Zare [e], Don A. Lucca [e], Michael Nastasi [a], Jian Wang [a, *]

[a] Mechanical and Materials Engineering, University of Nebraska-Lincoln, Lincoln, NE, 68588, USA
[b] Key Laboratory of Aerospace Materials and Performance (Ministry of Education), School of Materials Science and Engineering, Beihang University, Beijing, 100191, China
[c] Department of Physics, South University of Science and Technology, Shenzhen, 518055, China
[d] Materials Science and Technology Division, Los Alamos National Laboratory, Los Alamos, NM, 87544, USA
[e] School of Mechanical and Aerospace Engineering, Oklahoma State University, Stillwater, OK, 74078, USA

HIGHLIGHTS

- Mechanical properties of amorphous SiOC were investigated by in-situ SEM compression.
- Irradiation increases both strength and plasticity by improving film quality.
- Microstructural homogeneous amorphous SiOC are intrinsically strong and deformable.

GRAPHICAL ABSTRACT

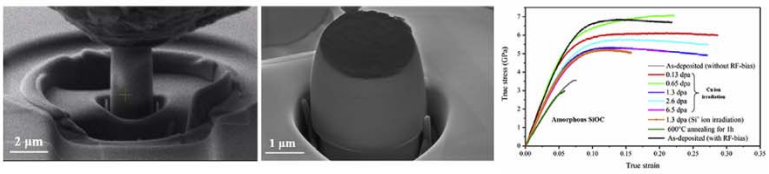

ARTICLE INFO

Article history:
Received 22 October 2018
Received in revised form
18 January 2019
Accepted 23 January 2019
Available online 25 January 2019

Keywords:
Silicon oxycarbide
Ion irradiation
Strength
Plasticity

ABSTRACT

Amorphous SiOC films were synthesized by magnetron sputtering at room temperature with/without radio frequency (RF) bias and further improved in terms of mechanical properties by ion irradiation. As-deposited SiOC films without RF bias exhibit catastrophic failure at a low stress and strain, which is ascribed to microstructural heterogeneities associated with the formation of voids during deposition, as evidenced by transmission electron microscopy. Ion irradiation unifies microstructure accompanied with eliminating the voids, resulting in a simultaneously increase in strength and plasticity (ultimate strength of 5–7 GPa and the strain to shear instability of over 20%). Homogeneous microstructures are demonstrated to ensure high strength and plasticity of amorphous SiOC, as observed in SiOC that are deposited with RF-bias. Thus, microstructural homogeneous amorphous SiOC exhibits intrinsically high strength and plasticity, making them promising as structural engineering materials.

1. Introduction

Amorphous silicon oxycarbide (SiOC) ceramics are a group of superior radiation-tolerant materials suitable for applications in reactor-like harsh environments due to their exceptional thermal stability and irradiation resistance [1–5]. SiOC ceramics can retain their amorphous structure without crystallization, void formation or segregation under ion irradiation doses up to 20 displacements per atom (dpa) at temperatures up to 600 °C [1,2,6–8]. Unlike crystalline solids, amorphous materials do not contain conventional crystal defects such as vacancies, interstitials or dislocations [9]. Therefore, highly stable amorphous SiOC ceramics are expected to eliminate the root cause responsible for irradiation damage in crystalline materials [2]. In addition, amorphous SiOC has been shown to have high crystallization temperatures (over 1300 °C), good oxidation and creep resistance [10–15]. Composite systems

* Corresponding author.
E-mail address: jianwang@unl.edu (J. Wang).

https://doi.org/10.1016/j.jnucmat.2019.01.035
0022-3115/

based on SiOC, such as amorphous-SiOC/crystalline-Fe nanostructures, show enhanced radiation-tolerance due to the presence of amorphous-crystalline interfaces which act as strong sinks for defects [16–22].

Strength and plasticity are of great importance for the successful application of radiation tolerant materials [23]. Previous studies have mainly focused on Young's modulus and hardness of SiOC using micro/nano-indentation tests [6,24,25]. It was found that irradiation leads to an apparent densification and a subsequent increase in elastic modulus and hardness of the SiOC [6,17,24]. The stress-strain behavior of the materials is rarely measured because of the complex stress/strain field underneath the indenter. Generally speaking, ceramic materials are believed to be hard and strong, but brittle due to the strong ionic and covalent bonds. However, recent studies show that nanoscale SiO_2 glass exhibit large homogeneous plastic strains in compression and superplastic elongation in tension at room temperature [26,27]. The SiO_4 tetrahedral unit that constitutes a continuous random network (CRN) in SiO_2 can easily tilt, which accommodates local mechanical strain. Because the SiOC CRN can be viewed as a SiO_2 CRN with some O atoms replaced by C [8,15,28–30], it is expected that amorphous SiOC ceramics should also be intrinsically deformable. Micro-compression, with the obvious advantage of a relatively uniform stress/strain field, is used to obtain the mechanical response of the amorphous SiOC films, i.e., the stress-strain relation.

The present work aims at determining intrinsic mechanical properties of amorphous SiOC films. To do so, we synthesize amorphous SiOC films by magnetron sputtering at room temperature, further modify microstructure through tailoring deposition conditions with/without radio frequency (RF) bias, or by heating or ion irradiation. Based on micro-pillar compression tests and microscopy characterization of these films, we conclude that amorphous SiOC is intrinsically strong and deformable which make them promising for structural engineering applications.

2. Experiments

Amorphous SiOC films were synthesized through radio frequency (RF) co-sputtering SiO_2 and SiC targets by magnetron sputtering techniques on to Si substrates with a top 300 nm SiO_2 layer. The sputtering deposition rates of SiO_2 and SiC used were 2:1, 1:1 and 1:2. The thickness of the as-deposited SiOC was approximately 4–5 μm. Additional amorphous SiOC films were deposited onto substrates under RF bias, with co-sputtering rates of SiO_2 and SiC at 1:1. Rutherford backscatter spectroscopy (RBS) analysis of the SiOC films with respect to the sputtering rates of SiC:SiO_2, 2:1, 1:1 and 1:2, confirms the compositions (at. %): Si-35.4%, C-32.9%, O-31.7%; Si-33.4%, C-21.6%, O-45.0%; and Si-29.6%, C-11.5%, O-58.9%, respectively [2]. As-deposited samples, with the sputtering rate of 1:1, were subjected to Cu ion irradiation to damage levels of 0.13, 0.65, 1.3, 2.6 and 6.5 dpa and Si ion irradiation to 1.3 dpa, and annealing in vacuum at 600 °C for 1 h. The depth-dependent damage and Cu concentration profiles were simulated by using the Stopping and Range of Ions in Matter (SRIM)-2008 software with the ion distribution and quick calculation of damage option using 15, 28, 28 eV for Si, C, and O [31]. Supplementary Fig. S1 presents the SRIM calculations of combined irradiation damage and depth profile of a series of Cu ion irradiation of different energies (1, 2, 3, 4, 5 MeV). The irradiation dose and corresponding irradiation damage are listed in Supplementary Table S1. Based on the SRIM calculation, the irradiation damages are approximately uniformly distributed throughout the top 3 μm films and less than 0.02 at.% Cu atoms are implanted. The irradiations were performed in the order of decreasing ion energy (the highest ion energy which results in the deepest ion end of range was irradiated first).

Nanoindentation was conducted to evaluate Young's modulus and hardness using a Hysitron TI950 nanoindenter with a diamond Berkovich tip and a cube corner tip. For the cube corner tip, the loading sequence consists of: 10 s loading to a maximum force of 10, 8, 6, 4, 2, 1, 0.5, and 0.1 mN → 60 s hold at the maximum force to allow any time dependent plastic effects to diminish → 5 s unloading to 10% of the maximum force → 60 s hold at 10% maximum force to measure thermal drift → 2 s final unloading. For the Berkovich tip, the load sequence is 5 s loading to a maximum force of 9, 8, 7, 6, 5, 4 and 3 mN → 2 s hold at the maximum force → 5 s unloading to 0 mN. The hardness and reduced modulus (E_r) were obtained from force vs. penetration depth curves [32]. The value of E_r is given by $1/E_r = (1- \nu^2)/E + (1- \nu_i^2)/E_i$, where E and ν are the elastic modulus and Poisson's ratio of the film, respectively. E_i and ν_i are the elastic modulus and Poisson's ratio of the indenter [32]. For a diamond indenter, $E_i = 1141$ GPa and $\nu_i = 0.07$ [33]. The Poisson's ratio of the SiOC film is 0.11 [34]. The elastic modulus of the SiOC can be calculated from the above equation. The average values of elastic modulus and hardness were obtained for 10 indentations along with their standard deviations. We obtain the similar values by using the two different tips (see Table 1 and Fig. S2 in the Supplementary materials). The indentation depth was maintained at less than 15% of the film thickness in order to minimizing the influence of substrate on the experimental results. The micro-pillars with diameters of 1–3.5 μm were machined from SiOC films by using focused ion beam methods. The height-to-diameter ratio of each pillar was 1–2. In situ scanning electron microscope (SEM) micro-compression tests were performed on micro-pillars at room temperature using a PI85 PicoIndenter (from Hysitron) with a flat punch diamond tip under displacement-control mode at displacement-control loading rates in the range of 5–500 nm/s. The cross-sectional SiOC films, before and after irradiation, were observed by transmission electron microscopy (TEM) (A FEI Tecnai G2 F20) coupled with energy dispersive spectroscopy (EDS). Specimens for TEM observation were made by grinding and polishing followed by low energy (3.5 keV) ion-milling.

3. Results

The mechanical behavior of the SiOC films was characterized using nanoindentation and in situ SEM micro-compression testing at room temperature. The displacement-control loading rate was 5 nm/s. The stress-strain curves were corrected by using the elastic modulus correction formula for a pillar [35]. The elastic modulus, with respect to the sputtering rate ratios of SiC:SiO_2, 2:1, 1:1 and 1:2, were 110.0 ± 3.3 GPa, 63.6 ± 2.8 GPa and 58.8 ± 0.6 GPa, respectively. Fig. 1(a) shows the true stress-strain curves of the

Table 1
Hardness and elastic modulus of the SiOC films, measured using a diamond Berkovich tip.

bm	Hardness (GPa)	Elastic modulus (GPa)
As-deposited (without RF-bias)	7.0 ± 0.8	63.6 ± 2.8
Cu^+: 0.13 dpa	12.6 ± 0.8	115.1 ± 3.0
Cu^+: 0.65 dpa	13.8 ± 1.5	126.2 ± 7.3
Cu^+: 1.3 dpa	9.5 ± 0.8	94.1 ± 4.8
Cu^+: 2.6 dpa	9.7 ± 0.2	100.2 ± 2.2
Cu^+: 6.5 dpa	9.2 ± 0.6	89.1 ± 5.5
Si^+:1.3 dpa	9.3 ± 1.3	91.2 ± 6.8
600 °C annealing for 1 h	7.3 ± 2.0	65.0 ± 3.0
As-deposited (with RF-bias)	12.0 ± 0.8	108.0 ± 5.6

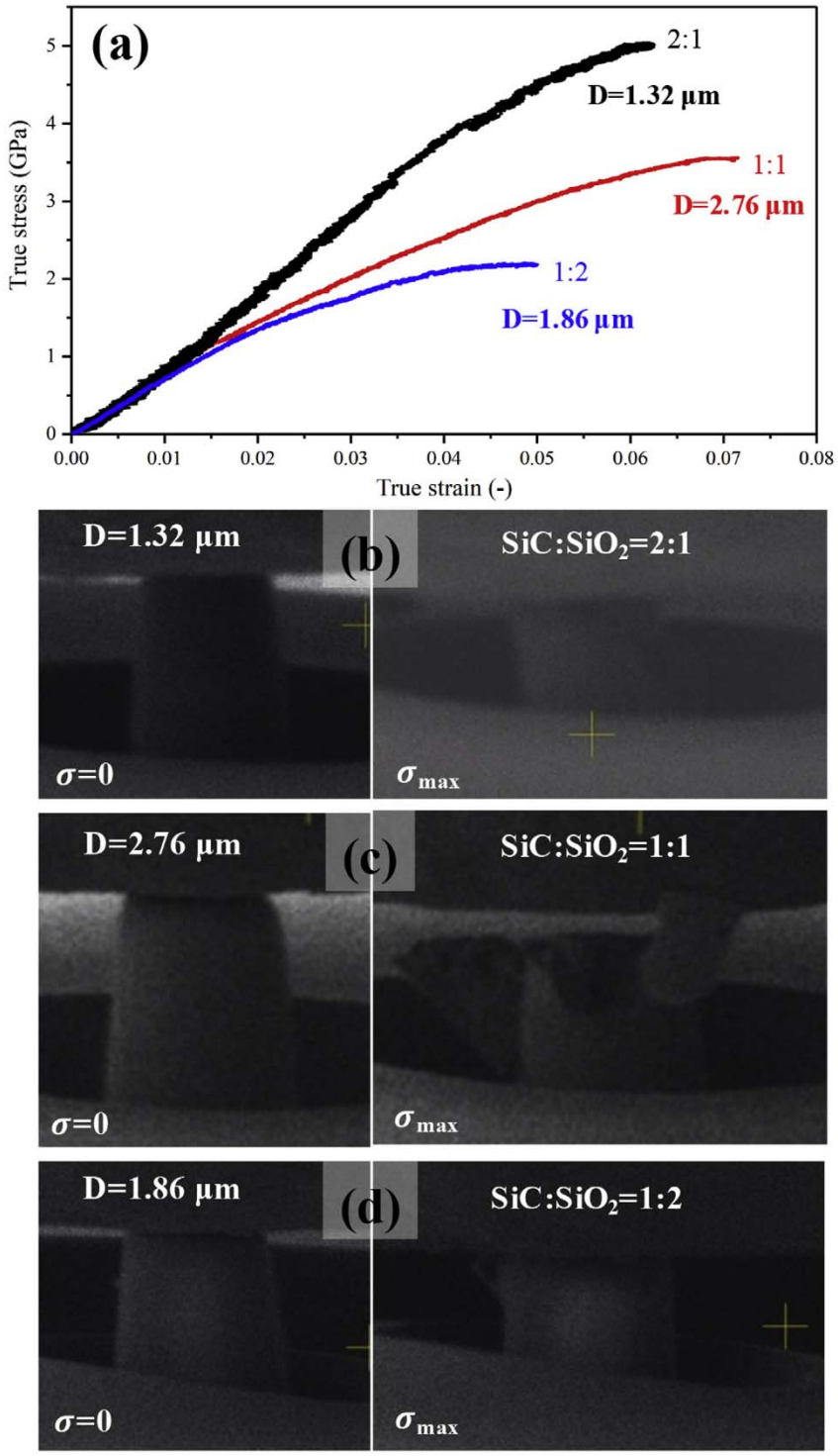

Fig. 1. (a) True stress-strain curves of the micro-pillars fabricated from as-deposited SiOC films (without RF-bias) with three different compositions. (b)–(d) The corresponding SEM images of the pillars before and after compression tests.

micro-pillars of as-deposited SiOC films without RF-bias with respect to the sputtering rate ratios of SiC:SiO_2, 2:1, 1:1 and 1:2. Fig. 1(b–d) shows the SEM images of as-deposited SiOC films before and after compression testing. The corresponding pillar diameter and compression strain are indicated in figures. Two important phenomena were observed. Micro-pillars were fractured abruptly at a strain of around 5%–7%, exhibiting typical brittle fracture, as shown in Fig. 1(b–d). The as-deposited SiOC sample at the deposition ratio of 1:1 shows a slightly large fracture strain. Therefore, further studies were performed on 1:1 amorphous SiOC.

Previous research suggested that the structural unit of SiOC amorphous ceramics is SiO_xC_{4-x} (x = 0,1,2,3,4) where silicon atoms are bonded to both carbon and oxygen atoms in a tetrahedral configuration [28]. Different compositions of SiOC films lead to various combinations and distributions of SiC_4, $SiOC_3$, SiO_2C_2, SiO_3C_1 and SiO_4 tetrahedra. In the C-free SiO_2 CRN, all tetrahedra have the same composition SiO_4 [36]. Despite the higher bonding energy of Si–O (800 kJ/mol) than that of Si–C (447 kJ/mol), the amorphous SiO_2 alloy exhibits a lower elastic modulus as compared to SiOC due to its low atomic packing density [34]. The higher elastic modulus of SiOC is probably due to the fact that Si–C bonds in SiOC CRNs can lead to a tighter, more closely packed structure [37]. The increasing elastic modulus and ultimate stress of the films with increasing C content is thus ascribed to the presence of Si–C bonds of the SiOC amorphous film.

Fig. 2 summarizes the hardness and elastic modulus of SiOC samples deposited with/without RF-bias and ion irradiated at different dpas. The as-deposited SiOC sample without RF-bias exhibits the lowest hardness and elastic modulus, around 7.0 ± 0.8 GPa and 63.6 ± 2.8 GPa, respectively. After Cu ion irradiation to damage levels of 0.13–6.5 dpa, both the hardness and elastic modulus increase significantly, showing obvious irradiation-induced hardening. For example, the 0.65 dpa irradiated samples exhibit the highest hardness (13.8 ± 1.5 GPa) and elastic modulus (126.2 ± 7.3 GPa). With further increase in irradiation dose from 0.65 dpa to 6.5 dpa, the hardness and elastic modulus decrease, but still remain higher than that of the as-deposited samples. The as-deposited SiOC sample with RF-bias possesses high hardness (12.0 ± 0.8 GPa) and elastic modulus (108.0 ± 5.6 GPa), which is much higher than that of the samples deposited without RF-bias. In addition, we also tested the effect of annealing on the mechanical properties of the as-deposited samples without RF-bias. The samples were annealed in vacuum at 600 °C for 1 h. The results show that annealing does not change the mechanical properties (see Fig. 2).

Besides the increase in elastic modulus and hardness, both strength and plasticity of SiOC amorphous films were significantly improved when they were synthesized by deposition with RF-bias or irradiated by Cu or Si ions. The samples deposited without RF-bias exhibit a low ultimate stress (~3.5 GPa) and a fracture strain of ~7%. Fig. 3(a) shows true stress-strain curves of micro-pillars in various states. The samples deposited with RF-bias display a high ultimate stress (~6.8 GPa) and a total strain of ~20% without fracture or cracking. Fig. 3(b) shows SEM images of the sample before and after compression. It is observed that there are no cracks and shear bands at the strain of 20%. When as-deposited samples (without RF-bias) were subjected to a Cu ion irradiation, there was a significant increase in both strength and plasticity as Cu ion irradiation to damage levels of 0.13–6.5 dpa. The irradiated samples display an ultimate stress of 5–7 GPa and total strains of over 20%, and exhibit homogeneous deformation without formation of shear bands (Fig. S3 in the Supplementary materials). The 0.65 dpa irradiated sample exhibited the highest strength (~7 GPa) and an obvious strain hardening effect. A typical pillar fabricated from the 0.65 dpa irradiated film before and after compression test is presented in

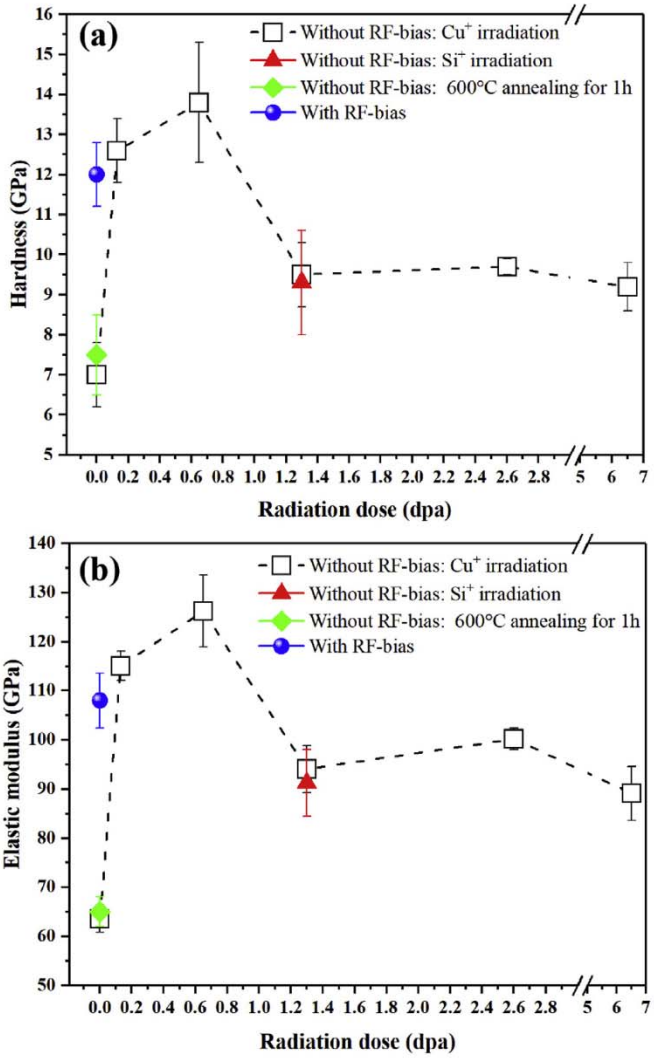

Fig. 2. (a) Hardness and (b) elastic modulus of the SiOC films deposited with/without RF-bias, ion irradiated at different dpas and after 600 °C annealing for 1 h. Indentation was conducted by using a diamond Berkovich tip.

Fig. 3(c), showing that the pillar was not fractured even though the compressive strains reached up to 23%. Instead, the pillar deformed homogeneously during compression without formation of shear bands, as evidenced by Fig. 3(d) which shows the shape of the irradiated pillar after compression to 23% of strain. The similar phenomena were observed in Si ion irradiated samples, as shown in Fig. 3(a) (also in Fig. S3 in Supplementary Materials). The SRIM simulation suggests that the Cu concentration in the Cu ion irradiated sample should be below 0.02 at.% (Fig. S1). This suggests that irradiation-induced strengthening was not due to the incorporation of Cu atoms in films. More importantly, ion irradiation is able to improve strength and plasticity of amorphous SiOC.

We also examine the stress-strain response at different strain rates. Fig. 4(a) shows the true stress-strain curves of 0.65 dpa ion irradiated samples at loading rates of 5 nm/s, 100 nm/s and 500 nm/s (corresponding to compression strain rates 1.25×10^{-3} s^{-1}, 2.5×10^{-2} s^{-1} and 1.25×10^{-1} s^{-1}). The results show little strain rate sensitivity. Fig. 4(b) and (c) show the SEM images of the irradiated pillars before and after compression tests with the loading rate of 100 nm/s. It was found that amorphous SiOC films can tolerate rapid deformation to a large strain without fracture or cracking.

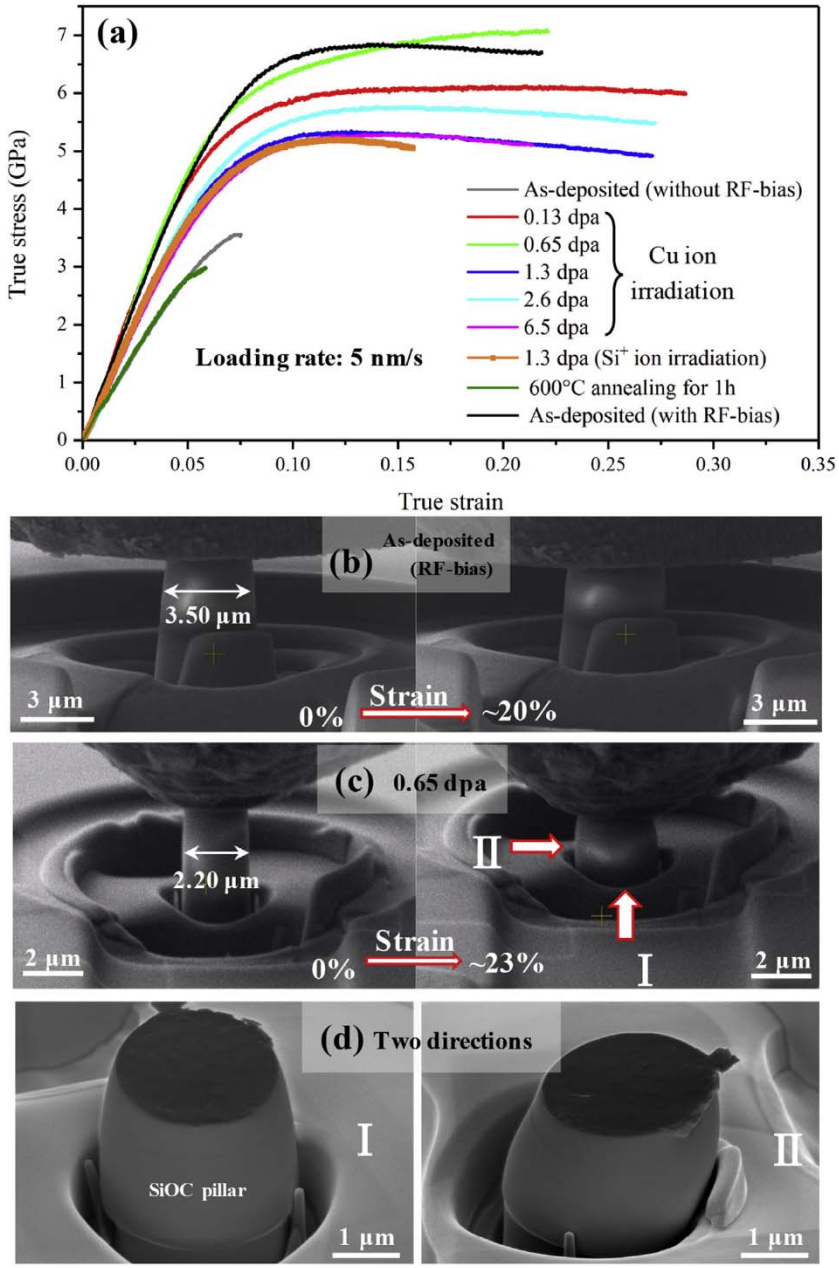

Fig. 3. (a) Comparison of true stress-strain curves of micro-pillars of SiOC films. SEM images of the pillars before and after compression test. (b) as-deposited pillar with RF-bias at a strain of ~20% and (c) 0.65 dpa irradiated pillar at a strain of ~23%. (d) SEM images of the 0.65 dpa irradiated pillar after a compression strain of ~23% observed along two directions I and II indicated in (c), showing the homogeneous deformation without formation of shear bands.

Fig. 4(d) and (e) are the SEM images of deformed samples from two directions, showing homogeneous deformation without formation of shear bands during the compression tests. Similarly, homogeneous deformation without formation of shear bands was also observed in irradiated samples after compressive deformation at loading rate of 500 nm/s, as shown in Fig. S4 in Supplementary Materials.

4. Discussion

Mechanical tests revealed improved mechanical properties of SiOC amorphous films that were ion irradiated or deposited with RF-bias. For amorphous alloys, it has been accepted that the low density or microstructure heterogeneity associated with formation of voids is responsible for low elastic modulus. The density of SiOC films deposited with RF-bias is around 2.5 g/cm^3 (determined by X-ray reflectivity), which is larger than that of the films deposited without RF-bias (2.2 g/cm^3). The increase in density is obviously attributed to the elimination of voids that can evolve due to shadowing effects during film deposition [38]. Here we characterize the microstructure of SiOC samples. Cross-sectional TEM micrographs of the as-deposited SiOC samples (without RF-bias) before and after Cu ion irradiation are shown in Fig. 5(a–c). The TEM bright-field (BF) images (Fig. 5(a_1), (b_1), (c_1)) were captured by using an over-focused condition, while Fig. 5(a_2), (b_2), (c_2) were captured by using under-focus. The TEM BF image of the as-deposited sample in Fig. 5(a_1) clearly shows many nano-sized black dots under the condition of over-focus. By tuning the focus

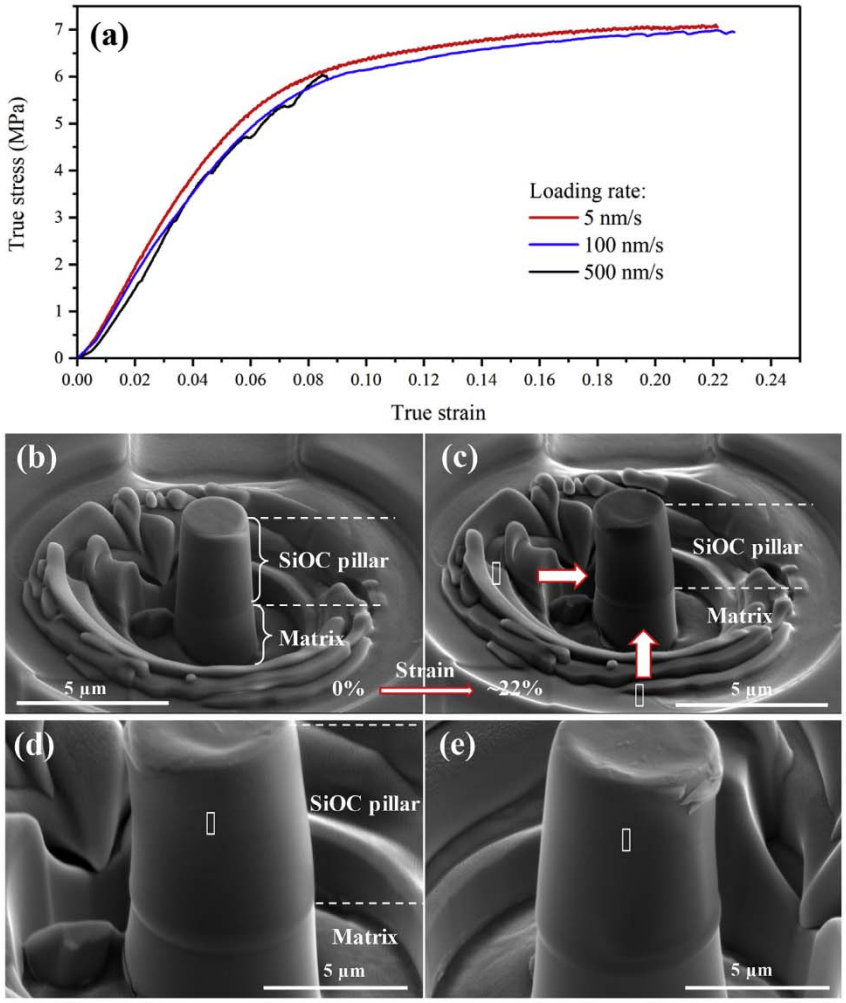

Fig. 4. (a) True stress-strain curves of the micro-pillars fabricated from as-deposited SiOC films (without RF-bias) after Cu ion irradiation to 0.65 dpa at different loading rates. (b) and (c) SEM images of the 0.65 dpa irradiated pillars before and after compression tests with the loading rate of 100 nm/s; (d) and (e) SEM images of the pillar observed from two directions indicated in (c), showing the homogeneous deformation without formation of shear bands.

to over-focus, we found that these black dots gradually transform into white dots, as shown in Fig. 5(a_2). This clearly demonstrates that many nano-scale voids formed in as-deposited SiOC films grown without RF-bias. After Cu ion irradiation to damage levels of 0.13 and 0.65 dpa (Fig. 5(b and c)), TEM BF images exhibit homogeneous contrast throughout the whole film without voids. The as-deposited samples after irradiation to higher damage levels of 1.3–6.5 dpa also exhibit homogeneous microstructures without any detectable voids. Signs of crystallization were not observed after exposure to damage levels of 0.13–6.5 dpa. The films retained their amorphous structure, as evidenced by the corresponding selected area electron diffraction patterns inserted in Fig. 5(a_2), (b_2), which is consistent with the previous reports [2]. Compared to ion irradiation, it was found that the application of an RF-bias to the substrate is another approach to improving the quality of the SiOC film. As shown in Fig. 5(d), the SiOC deposited with RF-bias exhibits a highly homogeneous microstructure without any discernible voids, which is quite different from the microstructure observed in the sample deposited without RF-bias (Fig. 5(a_1), (a_2)).

The influence of ion irradiation on the SiOC microstructure is demonstrated more clearly in Fig. 6. Fig. 6(a), which is a TEM BF image of the amorphous SiOC after partial irradiation using Cu ion, showing two different microstructures. The unirradiated region displays heterogeneous contrast with many nano-sized voids. By contrast, the irradiated region exhibits uniform contrast without voids. This indicates that ion irradiation can effectively heal the voids formed during the deposition process. Fig. 6(b) shows a scanning TEM image of the unirradiated region in SiOC and corresponding elemental mapping, revealing a significant lack of Si and O in black regions while there is a homogeneous distribution away from the void. This further confirms the presence of voids in as-deposited SiOC samples deposited without RF-bias.

Ion irradiation in SiOC may destroy high energy Si–O bonds and lead to formation of more Si–C bonds with low bonding energy. Indeed, it has been reported that ion irradiation results in a decreased number of Si–O bonds and an increased number of Si–C and C–O bonds in SiOC films [7]. In addition, more Si–C bonds are expected to form in SiOC with randomly dispersed C as compared to SiOC with aggregated C. It is conceivable that the irradiation-induced strengthening observed in present SiOC films can be attributed to an increase in Si–C bonds. The present work suggests that a 0.65 dpa irradiation is sufficient to destroy Si–O bonds and uniformly redistribute C atoms, because mechanical properties don't continuously increase as the irradiation exceeds 0.65 dpa. When the number of C–O bonds overtakes the number of Si–C bonds with continuous radiation (exceeding 0.65 dpa in the present SiOC film), the softening begins to occur. Note that annealing at 600 °C (well below crystallization temperature) does not destroy

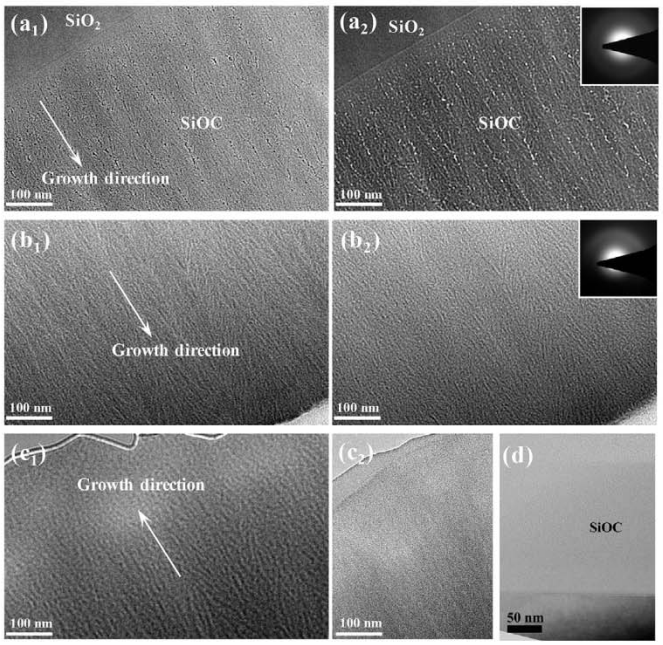

Fig. 5. Microstructures of SiOC samples that are deposited with/without RF-bias and after Cu ion irradiation. (a_1, a_2) Cross-sectional TEM micrographs of the SiOC samples deposited without RF-bias. (b_1, b_2) and (c_1, c_2) Cross-sectional TEM micrographs of the SiOC samples deposited without RF-bias after Cu ion irradiation to damage levels of 0.13 dpa and 0.65 dpa, respectively. (a_1, b_1, c_1) are captured over-focus, while (a_2, b_2, c_2) are captured under-focus. Some heterogeneity (such as voids) is observed in as-deposited sample. Irradiated sample shows homogeneous microstructure. (d) TEM image of the SiOC deposited with RF-bias, showing highly homogeneous microstructure without detectable voids.

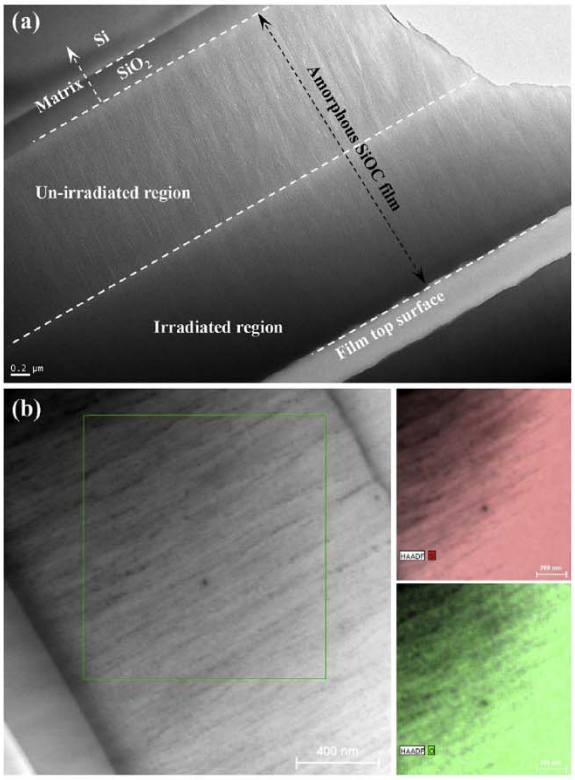

Fig. 6. (a) TEM image of the partially irradiated SiOC sample with the thickness of 3.5 μm, showing different contrast in irradiated and unirradiated regions. (b) A scanning TEM BF image of the unirradiated region in as-deposited SiOC film (without RF-bias) and corresponding Si (pink) and O (green) elements mapping in the outlined region, revealing significant lack of Si and O in black regions while homogeneous distribution in another region. (For interpretation of the references to colour in this figure legend, the reader is referred to the Web version of this article.)

Si—O bonds and redistribute C atoms, and cannot unify microstructure of as-deposited amorphous films. Thus, annealing at low temperature did not influence the mechanical properties of SiOC amorphous films (Fig. 3(a)).

The microstructural homogeneous amorphous SiOC (without voids and columnar structure) exhibits good plasticity. The good plasticity may originate from Si—O bonds in SiOC CRNs. It has been reported that amorphous SiO_2 materials exhibit excellent plasticity because their SiO_4 tetrahedral unit can be easily tilted by bond-switching events which accommodate local strain in SiO_2 [26,27]. The amorphous SiOC can be considered as a C-doped amorphous SiO_2 with C replacing some O atoms [28]. The exceptional intrinsic plasticity of amorphous SiOC films may originate from the bonding breaking and bonding-switching processes that mediate the rotation and migration of atomic clusters under high stresses.

5. Conclusion

Mechanical tests and microstructural characterizations of amorphous SiOC films revealed that microstructural heterogeneities, such as voids that developed during deposition, significantly degenerate mechanical properties of amorphous ceramics. Taking amorphous SiOC films as example, we demonstrated that microstructural homogeneity ensures intrinsically high strength and plasticity of amorphous SiOC, in contrast to the conventional concepts which generally believe that ceramic materials are inherently strong but brittle due to the rigid covalent or ionic bonds. The microstructural heterogeneities can be diminished by RF-bias assisted sputtering techniques or ion irradiation. Low temperature annealing (lower than recrystallization temperature) does not really modify microstructure developed during deposition. This work suggests that, in addition to being a promising radiation-tolerant material, the intrinsically ultra-high strength and excellent plasticity also make amorphous SiOC promising for structural engineering applications.

Acknowledgements

We acknowledge the partial financial support from the Department of Energy (DOE) Office of Nuclear Energy and Nuclear Energy Enabling Technologies through Award No. DE-NE0000533, and from the Nebraska Public Power District through the Nebraska Center for Energy Sciences Research at the University of Nebraska-Lincoln. The research was performed in part in National Nanotechnology Coordinated Infrastructure and the Nebraska Center for Materials and Nanoscience, which are supported by the National Science Foundation under Award ECCS: 1542182 and the Nebraska Research Initiative. Ion irradiation was performed at the Center for Integrated Nanotechnologies, an Office of Science User Facility operated for the U.S. DOE Office of Science. Los Alamos National Laboratory, an affirmative action equal opportunity employer, is operated by Los Alamos National Security, LLC, for the National Nuclear Security Administration of the U.S. Department of Energy under contract DE-AC52-06NA25396.

Appendix A. Supplementary data

Supplementary data to this article can be found online at https://doi.org/10.1016/j.jnucmat.2019.01.035.

References

[1] J.A. Colón Santana, E.E. Mora, L. Price, R. Balerio, L. Shao, M. Nastasi, Synthesis, thermal stability and the effects of ion irradiation in amorphous Si–O–C alloys, Nucl. Instrum. Methods B 350 (2015) 6–13.

[2] M. Nastasi, Q. Su, L. Price, J.A. Colón Santana, T. Chen, R. Balerio, L. Shao, Superior radiation tolerant materials: amorphous silicon oxycarbide, J. Nucl. Mater. 461 (2015) 200–205.

[3] Q. Su, B. Cui, M.A. Kirk, M. Nastasi, Cascade effects on the irradiation stability of amorphous SiOC, Phil. Mag. Lett. 96 (2) (2016) 60–66.

[4] P. Colombo, G. Mera, R. Riedel, G.D. Sorarù, Polymer-derived ceramics: 40 Years of research and innovation in advanced ceramics, J. Am. Ceram. Soc. 93 (7) (2010) 1805–1837.

[5] M. Mehregany, C.A. Zorman, N. Rajan, C.H. Wu, Silicon carbide MEMS for harsh environments, Proc. IEEE 86 (8) (1998) 1594–1609.

[6] Q. Su, S. King, L. Li, T. Wang, J. Gigax, L. Shao, W.A. Lanford, M. Nastasi, Microstructure-mechanical properties correlation in irradiated amorphous SiOC, Scripta Mater. 146 (2018) 316–320.

[7] Q. Su, S. Inoue, M. Ishimaru, J. Gigax, T. Wang, H. Ding, M.J. Demkowicz, L. Shao, M. Nastasi, Helium irradiation and implantation effects on the structure of amorphous silicon oxycarbide, Sci. Rep. 7 (1) (2017) 3900.

[8] C.G. Pantano, A.K. Singh, H. Zhang, Silicon oxycarbide glasses, J. Sol. Gel Sci. Technol. 14 (1) (1999) 7–25.

[9] P. Chaudhari, F. Spaepen, P.J. Steinhardt, Defects and atomic transport in metallic glasses, in: H. Beck, H.-J. Güntherodt (Eds.), Glassy Metal II: Atomic Structure and Dynamics, Electronic Structure, Magnetic Properties, Springer Berlin Heidelberg, Berlin, Heidelberg, 1983, pp. 127–168.

[10] G.D. Sorarù, D. Suttor, High temperature stability of sol-gel-derived SiOC glasses, J. Sol. Gel Sci. Technol. 14 (1) (1999) 69–74.

[11] R. Harshe, C. Balan, R. Riedel, Amorphous Si(Al)OC ceramic from polysiloxanes: bulk ceramic processing, crystallization behavior and applications, J. Eur. Ceram. Soc. 24 (12) (2004) 3471–3482.

[12] G.D. Sorarù, E. Dallapiccola, G. D'Andrea, Mechanical characterization of sol–gel-derived silicon oxycarbide glasses, J. Am. Ceram. Soc. 79 (8) (1996) 2074–2080.

[13] T. Rouxel, G.-D. Soraru, J. Vicens, Creep viscosity and stress relaxation of gel-derived silicon oxycarbide glasses, J. Am. Ceram. Soc. 84 (5) (2001) 1052–1058.

[14] T. Rouxel, G. Massouras, G.-D. Sorarù, High temperature behavior of a gel-derived SiOC glass: elasticity and viscosity, J. Sol. Gel Sci. Technol. 14 (1) (1999) 87–94.

[15] G.D. Sorarù, S. Modena, E. Guadagnino, P. Colombo, J. Egan, C. Pantano, Chemical durability of silicon oxycarbide glasses, J. Am. Ceram. Soc. 85 (6) (2002) 1529–1536.

[16] Q. Su, M. Zhernenkov, H. Ding, L. Price, D. Haskel, E.B. Watkins, J. Majewski, L. Shao, M.J. Demkowicz, M. Nastasi, Reaction of amorphous/crystalline SiOC/Fe interfaces by thermal annealing, Acta Mater. 135 (2017) 61–67.

[17] A. Zare, Q. Su, J. Gigax, S.A. Shojaee, M. Nastasi, L. Shao, D.A. Lucca, Effects of ion irradiation on structural and mechanical properties of crystalline Fe/amorphous SiOC nanolaminates, Acta Mater. 140 (2017) 10–19.

[18] Q. Su, B. Cui, M.A. Kirk, M. Nastasi, In-situ observation of radiation damage in nano-structured amorphous SiOC/crystalline Fe composite, Scripta Mater. 113 (2016) 79–83.

[19] Q. Su, F. Wang, B. Cui, M.A. Kirk, M. Nastasi, Temperature-dependent ion-beam mixing in amorphous SiOC/crystalline Fe composite, Mater. Res. Lett. 4 (4) (2016) 198–203.

[20] Q. Su, L. Price, J.A. Colon Santana, L. Shao, M. Nastasi, Irradiation tolerance of amorphous SiOC/crystalline Fe composite, Mater. Lett. 155 (2015) 138–141.

[21] Q. Su, J. Jian, H. Wang, M. Nastasi, Thermal stability of amorphous SiOC/crystalline Fe composite, Philos. Mag. A 95 (34) (2015) 3876–3887.

[22] Q. Su, L. Price, L. Shao, M. Nastasi, High temperature radiation responses of amorphous SiOC/crystalline Fe nanocomposite, J. Nucl. Mater. 479 (2016) 411–417.

[23] Y. Katoh, Q. Huang, Y.-H. Han, S. Risbud, Viewpoint set on nuclear materials science, Scripta Mater. 143 (2018) 126–128.

[24] S. Shojaee, Y. Qi, Y. Wang, A. Mehner, D. Lucca, Ion irradiation induced structural modifications and increase in elastic modulus of silica based thin films, Sci. Rep. 7 (2017) 40100.

[25] P. Du, X. Wang, I.K. Lin, X. Zhang, Effects of composition and thermal annealing on the mechanical properties of silicon oxycarbide films, Sensor. Actuat. A-Phys. 176 (2012) 90–98.

[26] K. Zheng, C. Wang, Y.Q. Cheng, Y. Yue, X. Han, Z. Zhang, Z. Shan, S.X. Mao, M. Ye, Y. Yin, E. Ma, Electron-beam-assisted superplastic shaping of nanoscale amorphous silica, Nat. Commun. 1 (2010) 24.

[27] J. Luo, J. Wang, E. Bitzek, J.Y. Huang, H. Zheng, L. Tong, Q. Yang, J. Li, S.X. Mao, Size-dependent brittle-to-ductile transition in silica glass nanofibers, Nano Lett. 16 (1) (2016) 105–113.

[28] H. Ding, M.J. Demkowicz, Hydrogen reverses the clustering tendency of carbon in amorphous silicon oxycarbide, Sci. Rep. 5 (2015) 13051.

[29] A. Saha, R. Raj, D.L. Williamson, A model for the nanodomains in polymer-derived SiCO, J. Am. Ceram. Soc. 89 (7) (2006) 2188–2195.

[30] H. Zhang, C.G. Pantano, Synthesis and characterization of silicon oxycarbide glasses, J. Am. Ceram. Soc. 73 (4) (1990) 958–963.

[31] J.F. Ziegler, The Stopping and Range of Ions in Solids, Ion Implantation Science and Technology, second ed., Elsevier, 1988, pp. 3–61.

[32] W.C. Oliver, G.M. Pharr, An improved technique for determining hardness and elastic modulus using load and displacement sensing indentation experiments, J. Mater. Res. 7 (6) (1992) 1564–1583.

[33] D.A. Lucca, K. Herrmann, M.J. Klopfstein, Nanoindentation: measuring methods and applications, CIRP. Ann. 59 (2) (2010) 803–819.

[34] T. Rouxel, Elastic properties and short-to medium-range order in glasses, J. Am. Ceram. Soc. 90 (10) (2007) 3019–3039.

[35] H.F.A. Abraham, Evaluation of micro-pillar compression tests for accurate determination of elastic-plastic constitutive relations, J. Appl. Mech. 79 (2012), 061011-1.

[36] S. Widgeon, S. Sen, G. Mera, E. Ionescu, R. Riedel, A. Navrotsky, 29Si and 13C solid-state NMR spectroscopic study of nanometer-scale structure and mass fractal characteristics of amorphous polymer derived silicon oxycarbide ceramics, Chem. Mater. 22 (23) (2010) 6221–6228.

[37] G.M. Renlund, S. Prochazka, R.H. Doremus, Silicon oxycarbide glasses: Part II. Structure and properties, J. Mater. Res. 6 (12) (1991) 2723–2734.

[38] M. Nastasi, N. Michael, J. Mayer, J.K. Hirvonen, M. James, Ion-solid Interactions: Fundamentals and Applications, Cambridge University Press, 1996.